Climate-informed stochastic hydrological modeling: Incorporating decadal-scale variability using paleo data

Benjamin J. Henley,[1] Mark A. Thyer,[2] George Kuczera,[1] and Stewart W. Franks[1]

Received 24 September 2010; revised 8 September 2011; accepted 22 September 2011; published 11 November 2011.

[1] A hierarchical framework for incorporating modes of climate variability into stochastic simulations of hydrological data is developed, termed the climate-informed multi-time scale stochastic (CIMSS) framework. A case study on two catchments in eastern Australia illustrates this framework. To develop an identifiable model characterizing long-term variability for the first level of the hierarchy, paleoclimate proxies, and instrumental indices describing the Interdecadal Pacific Oscillation (IPO) and the Pacific Decadal Oscillation (PDO) are analyzed. A new paleo IPO-PDO time series dating back 440 yr is produced, combining seven IPO-PDO paleo sources using an objective smoothing procedure to fit low-pass filters to individual records. The paleo data analysis indicates that wet/dry IPO-PDO states have a broad range of run lengths, with 90% between 3 and 33 yr and a mean of 15 yr. The Markov chain model, previously used to simulate oscillating wet/dry climate states, is found to underestimate the probability of wet/dry periods >5 yr, and is rejected in favor of a gamma distribution for simulating the run lengths of the wet/dry IPO-PDO states. For the second level of the hierarchy, a seasonal rainfall model is conditioned on the simulated IPO-PDO state. The model is able to replicate observed statistics such as seasonal and multiyear accumulated rainfall distributions and interannual autocorrelations. Mean seasonal rainfall in the IPO-PDO dry states is found to be 15%–28% lower than the wet state at the case study sites. In comparison, an annual lag-one autoregressive model is unable to adequately capture the observed rainfall distribution within separate IPO-PDO states.

Citation: Henley, B. J., M. A. Thyer, G. Kuczera, and S. W. Franks (2011), Climate-informed stochastic hydrological modeling: Incorporating decadal-scale variability using paleo data, *Water Resour. Res., 47*, W11509, doi:10.1029/2010WR010034.

1. Introduction

[2] Globally, water supply systems are becoming increasingly more vulnerable to the combined effects of climate variability, increasing water demand from growing populations [*Vörösmarty et al.*, 2000], and climate change. The management of these systems requires a reliable estimation of water supply drought risk, with stochastic models playing a key role when undertaking Monte Carlo simulations to estimate such a drought risk.

[3] Much work has been done to improve the ability of stochastic models to reproduce the observed statistics of hydrological records including both parametric and nonparametric approaches [*Salas*, 1993; *Koutsoyiannis*, 2000; *Frost et al.*, 2007; *Samuel and Sivapalan*, 2008; *Sharma et al.*, 1997; *Mehrotra and Sharma*, 2007]. However, most of these stochastic models have neglected valuable climate information.

[4] The Australian climate is influenced by large-scale ocean-atmosphere climate mechanisms such as the El Niño-Southern Oscillation (ENSO) [*McBride and Nicholls*, 1983; *Allan et al.*, 1996], the Interdecadal Pacific Oscillation (IPO) [*Power et al.*, 1999; *Folland et al.*, 2002], the Pacific Decadal Oscillation (PDO) [*Zhang et al.*, 1997; *Mantua et al.*, 1997], the Indian Ocean Dipole (IOD) [*Saji et al.*, 1999], and the Southern Annular Mode (SAM) [*Meneghini et al.*, 2007]. The variability explained by these mechanisms presents a valuable means for improving the ability of stochastic models to characterize temporal and spatial hydrological behavior. Interdecadal variability is increasingly seen as an important mode of variability in the climate system [*Arblaster et al.*, 2002]. Persistent periods of widespread rainfall deficit in the historical record underline the importance of interannual [*Hendon et al.*, 2007; *Ummenhofer et al.*, 2009] to interdecadal [*Arblaster et al.*, 2002; *Speer*, 2008] variability.

[5] *Meinke et al.* [2005] identified the effect of global-scale climate variability on rainfall variability at a range of timescales. The frequency component consistent with ENSO (2.5–8.0 yr) was found to account for most of the annual rainfall variability. Decadal (9–13 yr) variability had a significant (but lesser) impact, and interdecadal (15–18 yr) variability also had a significant (but lesser again) impact. For a detailed account of natural variability in the climate system at decadal and multidecadal timescales and the dominant climate change background signal, see *Parker et al.* [2007].

[6] Of importance for Australian water resource managers, is that most of the global annual rainfall variability at frequencies lower than ENSO was found in the study by

[1]Discipline of Civil, Surveying and Environmental Engineering, University of Newcastle, Callaghan, Australia.
[2]School of Civil, Environmental and Mining Engineering, University of Adelaide, Australia.

0043-1397/11/2010WR010034

Meinke et al. [2005] to occur in the Australasian region, in particular, the eastern half of the Australian continent. Water supply reservoirs typically have sufficient carry-over storage to maintain supply through shorter (e.g., El Niño) drought spells with run lengths up to 12–18 months, but are usually not designed to cope with decadal-scale dry periods. Low inflows associated with longer drought sequences present a greater challenge to environmental and water resource managers than shorter-lived events [*McGowan et al.*, 2009]. *Verdon et al.* [2004] demonstrated the impacts of ENSO and the IPO on rainfall on the east coast of Australia. The evidence of low frequency rainfall variability and the vulnerability of water supply systems to prolonged drought sequences prompt the need for a better understanding of this variability. Understanding low frequency variability in the climate system also has an important role in acting as a baseline against which climate change scenarios can be compared.

[7] Most hydroclimatic data records in Australia are 100–150 yr in length. *Thyer et al.* [2006] found that such records are too short to identify suitable stochastic models to simulate decadal- to multidecadal-scale variability without producing large uncertainty in the results. It follows that non-hydrological data such as indices of climate mechanisms may provide more information on persistent anomalous behavior of hydrological regimes. Paleoclimate records can provide further information to help improve certainty in light of short instrumental climate records.

[8] This paper focuses on modeling the decadal- to multidecadal-scale variability identified from observed paleoclimate IPO and PDO records in the context of the impact on water supply systems in Australia. The indices describing the PDO and the IPO phenomena relate to different regions of the Pacific Ocean. The PDO index is typically defined using North Pacific sea surface temperature (SST) data [*Mantua et al.*, 1997], while the IPO phenomenon is often described as a Pacific-wide manifestation of the PDO [*Power et al.*, 1999; *Folland et al.*, 2002]. The IPO and smoothed PDO indices are highly correlated (correlation = 0.86). Therefore, for this study it is assumed that the IPO and PDO indices represent the same broad pattern of variability and the phenomena in this study will be referred to collectively as the IPO-PDO phenomenon, except where reference to individual indices is required.

[9] Most stochastic hydrological models are conditioned only on observed rainfall or streamflow data. The lag-one autoregressive (AR(1)) model continues to be used widely by the water resources industry for stochastic rainfall simulations [*Thyer and Kuczera*, 2000]. Some models such as the hidden Markov model (HMM) of *Thyer and Kuczera* [2000] have conceptually incorporated mechanisms that describe long-term climate variability. However, they are limited in that they rely on instrumental rainfall and streamflow records. *Thyer et al.* [2006] suggested that climate/paleo data be used to better identify longer-term variability.

[10] There have been relatively few stochastic hydrological models that explicitly incorporate simulations of climate mechanisms using climate data, and none to date have incorporated parameter uncertainty. Drought risk can be significantly underestimated by approaches that ignore parameter uncertainty [*Stedinger and Taylor*, 1982; *Frost et al.*, 2007]. *Whiting et al.* [2003] used a regression approach to relate indices for the PDO and the ENSO to point rainfall and *Kiem and Franks* [2004] investigated the effect of the IPO on water supply drought risk. *Samuel and Sivapalan* [2008] used a Markov chain model to obtain stochastic sequences of IPO and ENSO states and incorporated the effects into a rainfall model.

[11] Few studies have collated information from multiple paleoclimate indices of the IPO-PDO. *Verdon and Franks* [2006] identified state changes of the PDO from several paleo sources, however, additional indices [*D'Arrigo and Wilson*, 2006; *Shen et al.*, 2006; *Linsley et al.*, 2008] will be used in this study. *Verdon and Franks* [2007] conditioned rainfall simulations on a "composite index" of the IPO, based on paleoclimate data. They simulated the run lengths of positive and negative states of the IPO with a log-normal distribution. However, a formal model selection procedure for the stochastic model used to simulate IPO-PDO state run lengths was not undertaken in any of the studies by *Samuel and Sivapalan* [2008], *Verdon and Franks* [2006], *Kiem and Franks* [2004], or *Whiting et al.* [2003].

[12] *Prairie et al.* [2008] calibrated a nonhomogeneous Markov model to the wet/dry hydrologic state from a paleo reconstruction of streamflow for the Colorado river, simulating streamflow using a *k*-nearest neighbor model conditioned on the hydrologic state. This approach offered a method to incorporate wet/dry hydrologic states guided by paleo data into a stochastic streamflow model. However, it relies exclusively on the availability of a site-specific streamflow paleo reconstruction and, moreover, did not undertake a formal model selection for the simulation of the hydrologic state.

[13] *Kwon et al.* [2009] used wavelet decomposition to isolate selected frequency components in climate proxies before simulating these components with autoregressive models. They then performed a regression of climate proxies against mean seasonal rainfall in South Florida to determine an appropriate subset of the proxies for use in the conditioning of a nonhomogeneous hidden Markov model (NHHM) of daily rainfall sequences. Their wavelet autoregressive modeling (WARM) approach for simulating frequency bands offers some promise in terms of a more explicit replication of variability over a particular range of timescales. However, there is considerable subjectivity in terms of the choice of the frequency bands. Moreover, the study by *Kwon et al.* [2009] did not investigate the ability of the WARM model to capture the observed statistics of the paleo/climate data. Another weakness of their approach is that the regression of climate proxies on the mean does not allow for the influence of climate on the variance of seasonal rainfall processes. *Kwon et al.* [2009] compared the observed wavelet power spectrum for Florida rainfall to the simulated spectra of the WARM-NHHM model and a simple AR(1) model on monthly data. The observed spectrum was found to be within the simulated 90% probability limits of both models. Their study also did not incorporate Pacific decadal-scale climate impacts, which is the focus of this paper.

[14] This paper presents a more comprehensive analysis than previous studies. It combines information from multiple paleo series in a thorough and objective manner to estimate the run length behavior of the IPO-PDO phenomenon. It undertakes a formal model selection process to identify a

stochastic model to simulate the IPO-PDO state run lengths. Furthermore, the influence of climate indices on additional seasonal rainfall characteristics, such as variance and skew, is included and parameter uncertainty is integrated into stochastic simulations of IPO-PDO states and seasonal rainfall.

[15] The key objective is to develop a climate-informed stochastic hydrological model (section 2). To achieve this objective, this study: (1) investigates the character of low frequency Pacific Ocean variability (IPO-PDO) using multiple sources of paleoclimate and instrumental data (section 3); (2) identifies a suitable stochastic model for low frequency Pacific Ocean variability for the purpose of simulating hydrological data (section 4); and (3) incorporates this new information into a stochastic model for hydrological data (section 5).

2. The General Hierarchical CIMSS Framework

[16] A Bayesian hierarchical approach for incorporating climate mechanisms and their effect on hydrological data is proposed, referred to here as the climate-informed multi-time scale stochastic (CIMSS) framework. Under this approach, physical phenomena operating at multiple timescales are simulated with stochastic models. In this study, the simplest form of the CIMSS model is adopted. It has a two level hierarchy, with the upper level simulating the wet/dry states of the IPO-PDO and the lower level simulating rainfall or streamflow, conditioned on the upper level. The upper level, level 0, contains a stochastic process for simulating the IPO-PDO, $y_t^0 \leftarrow p(y^0|Y_{t-1}^0, \theta^0)$. The simulated value at time step t, y_t^0 is drawn from a stochastic process conditioned on previous simulated data $Y_{t-1}^0 = [y_1^0, y_2^0, \ldots, y_{t-1}^0]$ where θ^0 are the level 0 model parameters. This model is developed in sections 3 and 4. The process at level 1 is conditioned on level 0, as in: $y_t^1 \leftarrow p(y^1|Y_{t-1}^1, \theta^1, y_t^0)$. The level 1 model is developed in section 5. Observed data is referred to in this study as Y_{obs}^0 (the IPO-PDO run lengths) and Y_{obs}^1 (the rainfall data).

3. Characterizing IPO-PDO Variability Using Paleo Data

[17] Given the hydrological impacts of modes of Pacific climate variability, the time within each IPO-PDO state is an important factor affecting water supply drought risk in the Pacific region. The term "run length" is used here to refer to the length of time between consecutive crossings, where a crossing is determined by a shift from the negative to positive state (or vice versa) with respect to the long-term median of the time series.

[18] The IPO index of *Power et al.* [1999] and *Folland et al.* [2002] exhibits eight positive and negative states in the 161-yr observed (partially instrumental, partially reconstructed) record from 1850–2010 (based on 11-yr low-pass Chebyshev filtered HadSST2 data [*Rayner et al.*, 2006], as in the work of *Parker et al.* [2007]). The observed run lengths range from 7 to 32 yr. So few instrumental realizations of IPO states induces large uncertainty about the run-length behavior of the IPO.

[19] Paleoclimate data provides a valuable source of information on the long-term behavior of IPO-PDO. *McGregor et al.* [2010] combined 10 ENSO paleo proxies and compared a 13-yr low-pass filtered version of their ENSO proxy with two PDO reconstructions [*Biondi et al.*, 2001; *D'Arrigo et al.*, 2001] and the IPO and PDO. A more direct approach to obtain a preinstrumental paleo IPO-PDO time series would be to directly combine the available IPO-PDO paleoclimate reconstructions, as is undertaken in this paper.

[20] To the best of the authors' knowledge, there are seven formally published paleoclimate indices for the PDO or the IPO. These paleo records, as described in Table 1, are from both the eastern and western sides of the Pacific basin and use tree rings, coral, and drought/flood index records. The correlation between the indices ranges between -0.02 and 0.75. Given the varying levels of agreement between signals, attempting to subjectively identify the precise history of state changes is likely to be problematic. A robust procedure to combine the signals and extract the run length behavior from the IPO-PDO paleo data sources is needed.

3.1. Previous Investigations Into Identifying Pacific Multidecadal Hydrological Variability

[21] Previously, *Verdon and Franks* [2006] identified step changes in both IPO and PDO paleo and instrumental data sources. They used the first four of the published paleo records in Table 1 and a coral record at Raratonga [*Linsley et al.*, 2000]. Their approach used the Mann-Whitney U-test to identify differences between two halves of data in a moving window. *Mauget* [2003] used a similar approach to detect intra- and multidecadal shifts in streamflow, precipitation, and temperature. However, a critically important issue

Table 1. Pacific Paleoclimate Indices, Mean Run Lengths for Shift Detection Tests[a]

Paleo Series	Proxy For	Length (yrs)	Location of Source	Weight	Mean Run Lengths		Order	Cutoff Period (yrs)
					10-yr window	40-yr window		
Biondi et al. [2001]	PDO	330	Southern and Baja California tree rings	0.14	8.2	35.6	8	19
D'Arrigo et al. [2001]	PDO	300	West-coast of North America tree rings	0.16	14.0	20.1	6	27
Gedalof and Smith [2001]	PDO	400	West-coast of North America tree rings	0.10	10.3	25.9	2	26
MacDonald and Case [2005]	PDO	1000	California and Alberta tree rings	0.10	9.6	24.9	8	19
D'Arrigo and Wilson [2006]	PDO	420	East Asia tree rings	0.17	12.1	17.0	2	14
Shen et al. [2006]	PDO	530	Eastern China drought/flood index records	0.13	25.2	26.6	2	19
Linsley et al. [2008]	IPO	350	Fiji/Tonga oxygen isotopes from coral cores	0.20	6.7	26.1	3	45
PDO (Instrumental)	-	107	Leading EOF of North Pacific SST	-	13.7	25.5	-	-
IPO (Instrumental)	-	158	Leading EOF of 11-yr filtered Pacific SST	-	11.3	18.0	-	-
Mean of paleo	-	-	-	-	12.3	24.4	-	-

[a]Tests were done using 10 and 40 yr windows and low-pass filter orders and cutoff periods.

arises: the decision of a suitable window length. *Verdon and Franks* [2006] used a subjective choice of 30 yr for the window length. Once the individual series of step changes was derived, further subjective choices were made to estimate the history of state shifts in IPO-PDO, despite the coherence between the state shifts being poor at several points in the records. *Tome and Miranda* [2005] recommend an adaptive technique for detecting continuous partial trends in the data. Their method required the user to input a minimum time (i.e., run length) between breakpoints, and relaxes this condition at the data boundaries. Related studies emphasize the need for care in the choice of smoothing filter/window width and the treatment of boundary constraints [*Soon et al.*, 2004; *Mann*, 2004, 2009; *Arguez et al.*, 2008]. *Mann* [2004] warns against false conclusions based on "unobjective" statistical smoothing approaches.

3.2. Sensitivity of Run lengths to the Choice of Shift Detection/Smoothing Window

[22] The sensitivity of run lengths to the choice of window width was investigated using the shift detection test as used by *Mauget* [2003] and *Verdon and Franks* [2006]. The test was applied to the seven paleo series and the instrumental PDO and IPO using a range of window widths (from 4 to 60 yr). The mean run length was found to be strongly dependent on the choice of window width; Table 1 shows the results for window widths of 10 and 40 yr. Similar tests using both moving-average smoothing and low-pass filters with a range of smoothing orders/cut-off periods produced similar results. The mean run lengths were strongly dependent on the smoothing order/cut-off period. It can be concluded that a subjective choice of window width/smoothing order/cut-off period, as used by *Verdon and Franks* [2006], with any of these three signal extraction techniques is likely to bias the results significantly. This motivates the development of a more objective method for identifying decadal-scale variability from paleo records.

3.3. Extracting the IPO-PDO Signal From the Paleo Records

[23] As well as low frequency (e.g., decadal/multidecadal) variability, the paleo records exhibit higher frequency variability, which is not typical of the IPO-PDO signature. This higher variability is likely due to the paleoclimate time series being based on proxies, which induce some additional noise. Despite these uncertainties, it is hypothesized that the IPO-PDO paleo records from multiple sources and locations (especially when combined) contain a robust representation of the IPO-PDO phenomenon. To extract the signal from the paleo records that is most similar to the instrumental IPO-PDO series, filtering is required to remove the noise and higher frequency variability.

3.3.1. Filtering the Paleo Records

[24] A low-pass Butterworth filter was used to filter each paleo index. The Butterworth filter was chosen because it has flatter frequency response in the passband than other filters, resulting in uniform treatment of the passband frequencies in the signal. However, the choice of filter is not considered to have as significant an impact on the results as the parameters of the filter. The filter parameters, the filter order (n), and the cut-off period (ω_c) were calibrated by maximizing the Nash-Sutcliffe efficiency (NSE) between the filtered paleo index and the instrumental IPO record during the instrumental period (1850–2008). Signals were standardized prior to calculation of the NSE. Parameter ranges of $n \in (2, 8)$ and $\omega_c \in (3, 50)$ were used. The fitted parameter values are shown in Table 3. Maximum NSE values range between -0.03 and 0.48, with a mean of 0.21. This technique removes noise from the paleo indices and preserves the signal within each reconstruction that provides the best fit to the IPO index during the instrumental period. This technique is less sensitive to assumptions about the frequency of state changes of the IPO-PDO than a subjective decision [e.g., *Verdon and Franks*, 2006], since the parameters are chosen using the best fit to the instrumental record.

3.3.2. Coherence of the Filtered Signals

[25] The coherence of the filtered indices was investigated by examining the cross-correlation coefficients between the filtered indices. During the instrumental (calibration) period, the values ranged from –0.32 to +0.84 (mean of +0.38); however, during the preinstrumental period the coherence was reduced, with cross-correlation coefficients varying between –0.43 and +0.35 (mean of –0.06). This is likely because (1) the IPO-PDO does not necessarily explain a large degree of the variability in the proxies (because of a range of independent regional and local effects, for example, orographic effects) and (2), the relationship between the climate phenomena and the predictor signal (tree ring width, oxygen isotopes from coral) is not necessarily time-invariant.

[26] To take account of the varying coherence during the instrumental period, a weighted average of the seven time series was computed to produce a combined paleo IPO-PDO signal (referred to hereafter as the CPIPO index). Before combining them, each filtered paleo time series was normalized so that its mean and standard deviation matched those of the instrumental IPO index. The weights used were proportional to the inverse of the error variance between the filtered paleo series and the instrumental IPO index. This is similar to the weighting method used in weighted least squares regression. This method assumes that the coherence is stationary throughout the preinstrumental and instrumental periods. This is discussed further in section 6. Table 1 shows the resulting weights for each paleo record.

[27] Figure 1 shows the CPIPO time series. The instrumental IPO index compares favorably with the new reconstruction (NSE = 0.75). The distribution of run lengths from the CPIPO is used to inform the model selection and calibration procedures in section 4.

4. Modeling the Run lengths Within States of the IPO-PDO

4.1. Distribution of Run lengths

[28] Figure 2 compares the smoothed empirical density of run lengths of the CPIPO signal to that of *Verdon and Franks* [2006]. There are marked differences between the two distributions. The subjective choice of window length (30 yr) and historical shifts in the paleo records by *Verdon and Franks* [2006] resulted in some sets of shorter runs, possibly being mistaken as single (longer) runs. As such, the run length distribution of *Verdon and Franks* [2006] appears to have been biased toward longer run lengths. The results of this study favor a considerably higher likelihood of run lengths under 10 yr: the proportion being 0.39, while in the

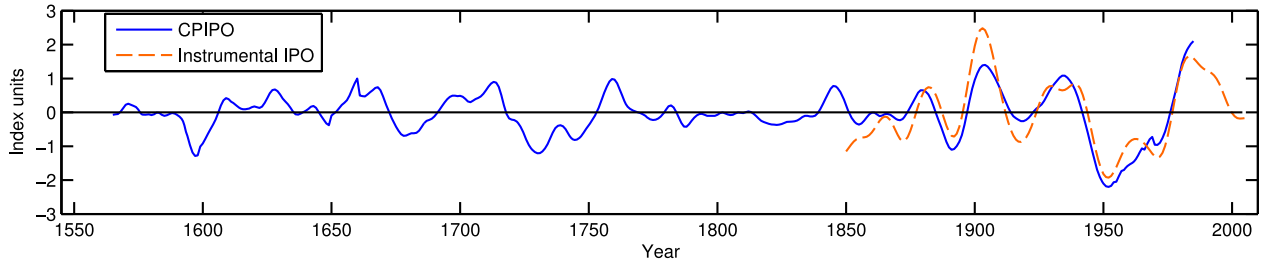

Figure 1. The combined paleo IPO-PDO and instrumental IPO time series.

Verdon and Franks [2006] study it was 0.05. The apparent bimodality of the empirical PDF is most likely because of sampling variability. Stationarity of the run lengths was investigated with a two-sided Kolmogorov-Smirnov (KS) test between the sets of run lengths in each century, with no statistically significant difference evident at the 5% level. Thus, no evidence was found to reject the assumption of stationarity of the run lengths between centuries.

4.2. Model Selection

[29] To simulate the run lengths of IPO-PDO states, it is necessary to identify the probability model that best fits the empirical distribution of run lengths shown in Figure 2. The candidate models were chosen either because they had been previously used to model long-term variability in hydrological data, or their probability density functions exhibit a similar shape to the empirical density in Figure 2. The run length models included the first- and second-order autoregressive (AR(1) and AR(2)) processes (calibrating the run length distribution, rather than the time series directly), the generalized extreme value (GEV) distribution, the truncated normal distribution with Box-Cox transformation (TN-BC), a two-state Markov chain model (MCM), the truncated normal (TN) distribution, the lognormal distribution as used by *Verdon* [2007], and the gamma distribution. The MCM has been widely used in stochastic hydrology to simulate the wet/dry behavior of climate [*Thyer and Kuczera*, 2003; *Lambert et al.*, 2003; *Akintug and Rasmussen*, 2005; *Frost et al.*, 2007; *Potter et al.*, 2010] and was used by *Samuel and Sivapalan* [2008] to simulate IPO states and by *Prairie et al.* [2008] to simulate wet/dry hydrologic states. The two-state MCM was fitted in the usual manner, by estimating the transition probabilities using $\hat{p}_{dw} = P(S_{t+1} = w|S_t = d) = n_{dw}/n_d$, where $\hat{p}_{dw}$ is the estimate of the probability (P) of a transition from a dry state ($S_t = d$) to a wet state ($S_{t+1} = w$), based on the number of transition years from dry to wet (n_{dw}) as a proportion of the total number of dry years (n_d) (similarly for the wet to dry transition probability). AR models have been used widely to simulate persistence and were used in the wavelet autoregressive model (WARM) by *Kwon et al.* [2009]. In this model selection all models were calibrated using the method of maximum likelihood. The AR models were calibrated by evaluating the likelihood of the observed paleo run lengths using the Monte Carlo simulated run length distribution for a given parameter set. The aim here is to determine if an AR lag combination can outperform the other distributions in terms of the Bayesian information criterion (BIC) based on the run lengths. Simulations from the continuous distributions were discretized to the annual time step during the simulation. A two-sided KS test between the observed run lengths indicated symmetry of the positive and negative runs (p = 0.77), so all models used a symmetrical distribution of runs in the two states.

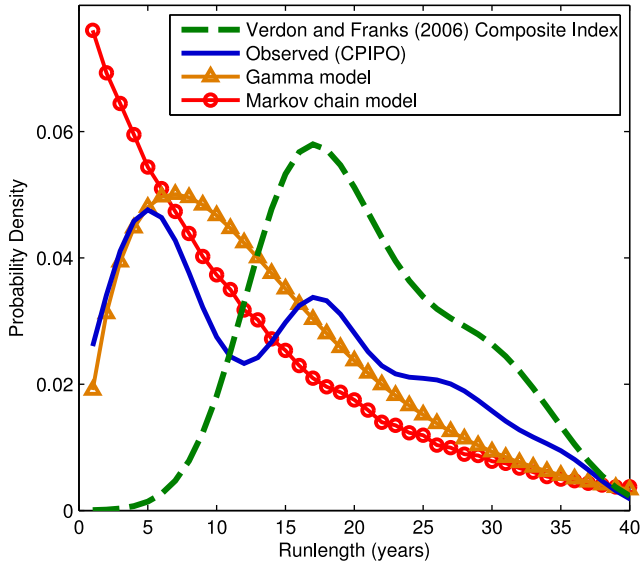

Figure 2. Observed and simulated IPO-PDO runlength distributions. The observed distributions include the composite index of *Verdon and Franks* [2006] and the CPIPO from this study (3-yr kernel smoothing window).

[30] The model selection was guided by the BIC of *Schwarz* [1978],

$$\mathrm{BIC} = -2 \ln L + k \ln n, \tag{1}$$

where L is the maximized value of the likelihood function after fitting the model, k is the number of fitted parameters, and n is the number of observations. A lower BIC value indicates a more favorable model. Figure 3 compares the BIC results for the calibrated models. The model with the lowest BIC was the gamma distribution. In addition, a two-sided KS test was performed to determine if the fitted gamma distribution provided a good fit to the observed data. The KS test showed no significant inconsistency between the observed and simulated data (p = 0.83). Consequently, the gamma model was adopted.

[31] Figure 2 compares the distribution of simulated runs for the MCM and gamma models against the observed CPIPO distribution. The MCM has a geometric probability density with its mode at a run length of 1 yr, quite unlike the observed data. Thus, it is structurally inappropriate for the simulation of quasiperiodic data such as the run lengths

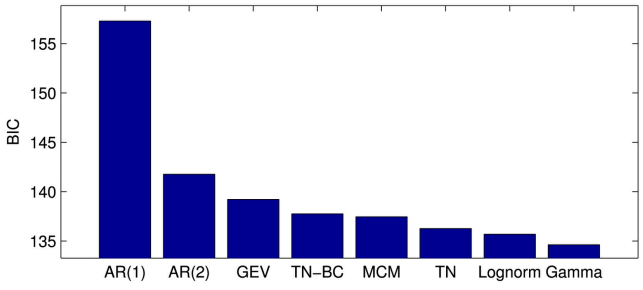

Figure 3. The BIC results for candidate IPO-PDO run-length models.

of the IPO-PDO. As demonstrated in Figure 2, the MCM overestimates the probability of shorter runs (e.g., 1–5 yr) and underestimates the probability of longer runs (e.g., >5 yr). It should be noted that a hidden Markov model calibrated to hydrological data alone would have the same shortcoming because the wet/dry state evolution is a Markov chain, and thus has the same monotonically decreasing run-length probability density. Thus, the gamma distribution for run lengths was found to provide the best fit (in terms of BIC) to the observed data.

4.3. Combining Paleo IPO-PDO and Instrumental IPO Information

[32] The paleo and instrumental data were combined to infer the posterior distribution of the parameters for the gamma model for the run lengths:

$$p(\theta^0|Y^0_{\text{obs,ins}}, Y^0_{\text{obs,pal}}) \propto p(Y^0_{\text{obs,ins}}, Y^0_{\text{obs,pal}}|\theta^0)p(\theta^0), \qquad (2)$$

where $\theta^0 = [\alpha, \beta]$, α (shape), and β (inverse scale) are the parameters of the gamma distribution, $Y_{\text{obs,pal}}$ represents the runs from the portion of the CPIPO in the preinstrumental period, $Y_{\text{obs,ins}}$ represents the runs in the instrumental period, and $p(\theta^0)$ is an uninformative prior. The posterior distribution in equation (2) was estimated using a Markov chain Monte Carlo (MCMC) method, the Metropolis algorithm (see section 5.4). Convergence was verified by checking that the average jump ratio and R-statistic were within ranges recommended by *Gelman et al.* [2004].

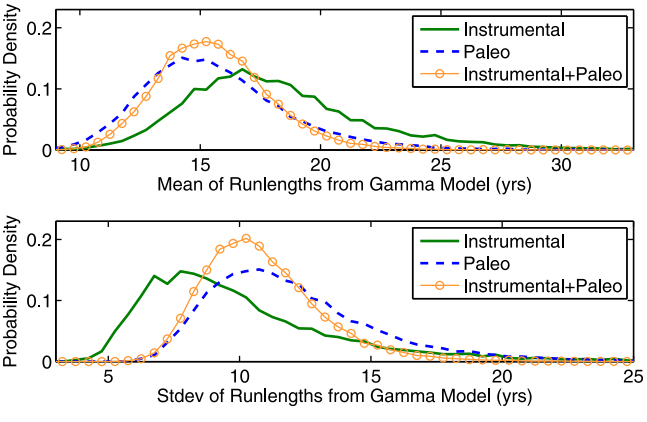

Figure 4. The posterior distributions of the mean and standard deviation of the gamma models calibrated to paleo, instrumental, and paleo plus instrumental IPO-PDO run lengths.

[33] Figure 4 compares the distribution of the mean (α/β) and the standard deviation ($\sqrt{\alpha}/\beta$) for the gamma model conditioned on the paleo, instrumental, and the paleo with instrumental (equation (2)) data. Incorporation of paleo information reduced the uncertainty in the run length mean and standard deviation; their posterior modes were 15.3 and 10.3 yr, respectively. The distributions of simulated IPO-PDO run lengths, with an allowance for uncertainty in α and β, are shown in Figure 5. The differences between the paleo and instrumental distributions could be attributable to the low number of samples in the instrumental period or the uncertainty of the paleo data. This is discussed further in section 6.2.

5. A Stochastic Model for Hydrological Data Incorporating Pacific Decadal Variability

[34] The CIMSS framework is illustrated for a case study modeling seasonal rainfall on the east coast of Australia. In section 5, the spatial and temporal influence of the IPO-PDO on rainfall is first investigated, then an appropriate stochastic hydrological model is developed. Following that, the calibration procedure is explained, and two location-specific case studies follow.

5.1. The Influence of the IPO-PDO on East Coast Australian Rainfall

[35] A number of studies have shown the influence of the IPO-PDO on Australian hydrological regimes, including: *Power et al.* [1999]; *Arblaster et al.* [2002]; *Kiem and Franks* [2004]; *Micevski et al.* [2006]; *Speer* [2008]; *Heinrich et al.* [2009]; *Verdon-Kidd and Kiem* [2009]; and *Westra and Sharma* [2009]. Figure 6 illustrates the spatial influence of the IPO-PDO state on mean annual rainfall for 1900–2007 for New South Wales (NSW, eastern Australia). The data used here is the gridded monthly rainfall data from the Bureau of Meteorology's (BOM) Australian Water Availability Project. The IPO-PDO negative state appears to coincide with higher annual rainfall over ~1000 km of the coast of NSW, extending inland ~100 km. Despite this consistent spatial impact on the mean rainfall, there remains much variability. Two point-rainfall case study sites are used in this study, Stroud and Cataract Dam, as detailed in Table 2. The data is from the BOM's high

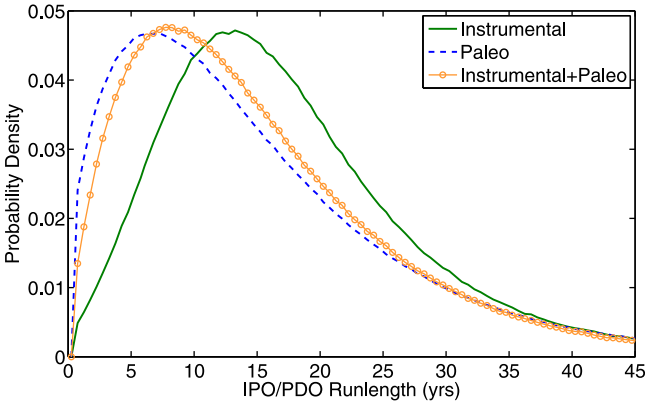

Figure 5. A comparison of the distributions of simulated IPO-PDO runs incorporating parameter uncertainty.

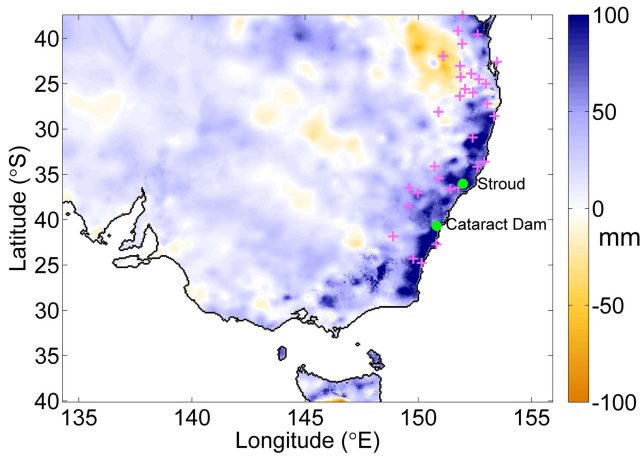

Figure 6. The difference in mean annual rainfall (calendar year) for IPO-PDO negative minus IPO-PDO positive years for 1900–2007 for NSW. Crosses indicate locations of coastal high-quality rain gages in NSW. The locations of the Stroud and Cataract Dam case study sites are shown.

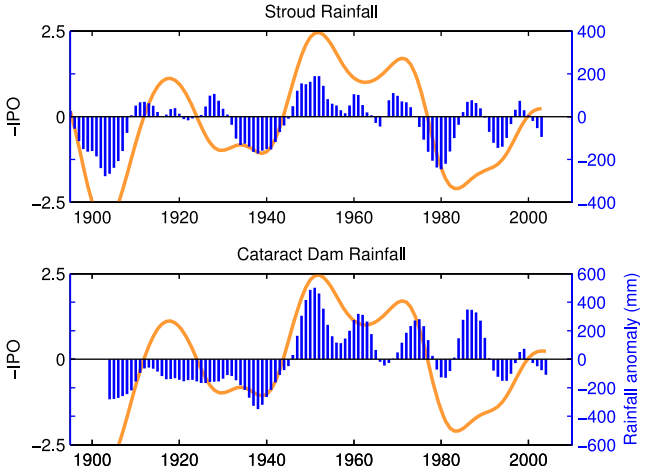

Figure 7. Smoothed (11-yr moving average) annual rainfall anomaly for Stroud and Cataract Dam (blue bars) and the instrumental IPO index (orange curve).

quality (HQ) rainfall data set [*Lavery et al.*, 1997]. Using a linear fit of the annual IPO index values to annual (calendar year) rainfall totals at two case study sites, the IPO-PDO explains only 10.5% and 4.7% of the total variance at Stroud and Cataract Dam, respectively. Figure 7 shows a time series of smoothed (11-yr moving average) annual rainfall anomalies at the two case study sites plotted with the instrumental IPO index. The shift to the negative IPO-PDO state in the mid 1940s coincides with an increase in rainfall at both sites. The opposite occurs when the IPO-PDO state shifts to its positive state in the late 1970s. The "Federation Drought" (~1900) and the "WWII Drought" (late 1930s–mid 1940s) are also visible in the smoothed rainfall anomalies. Anomalies of the order of 200–400 mm (the case study sites both have mean annual rainfall of ~1000–1100 mm) appear to be quite closely associated with the state of the IPO-PDO, despite the low proportion of rainfall variance explained by annual IPO index values. Some effects appear to be contrary to this (e.g., pre-1930 and post-1985 rainfall at Cataract Dam), which could be due to the influence of other climate mechanisms. Despite this, the results indicate that the IPO-PDO has a consistent and broad impact on rainfall over a significant region along the NSW coast.

5.2. Investigating the Temporal Impact of the IPO

[36] Figure 8 shows the influence of the IPO-PDO on monthly rainfall statistics at the two case study sites. The impact appears strongest for the summer months, with some impacts also evident in June. To investigate whether or not these results were specific to the case study sites only, an analysis of the monthly and seasonal influence of the IPO-PDO was undertaken for the 47 BOM HQ rainfall data sites on the east coast of Australia (the locations of the NSW sites are shown in Figure 6). The nonparametric Wilcoxon rank-sum test was used to test for significant differences between seasonal rainfall totals in the IPO-PDO positive and negative states at the 95% significance level. Tests were performed on rainfall totals in all possible contiguous monthly sequences (seasons) for all 47 sites. This included season durations from 1 to 12 months starting from January to December, yielding a total of 144 possible impact seasons. All but eight of the 47 sites exhibited statistically significant differences between IPO-PDO positive and negative states. The maximum impact seasons (minimum p-value) varied in duration somewhat, but were generally centered around the Austral summer, with some statistically significant impacts observed at other times of the year. Other conventions for the impact season could be used in simulations, for example, the longest statistically significant impact season, however, this is left for future work. The maximum impact seasons for the Stroud and Cataract Dam rainfall sites are shown in Table 2.

5.3. Seasonal Stochastic Model to Incorporate the Influence of the IPO-PDO

[37] The general CIMSS framework allows for the incorporation of the decadal-scale climate variability of the IPO-PDO, using the model identified for level 0 of the framework in section 4.2, into stochastic simulations of rainfall data at a single site. In this implementation, the IPO-PDO influences the rainfall during the impact season, as defined by the user, with the aid of a seasonal analysis such as that described in section 5.2. Impact and nonimpact seasons were modeled independently. This model structure was based on analysis of the case study data, which showed statistically significant correlations between consecutive impact seasons and between consecutive nonimpact seasons, but

Table 2. Rainfall Data and IPO-PDO Impact Seasons

Site Name	Data Type	Dates	Time Resolution	IPO-PDO Max Impact
Stroud post office	Rainfall	1889–2004	Monthly	January–March
Cataract Dam	Rainfall	1904–2005	Monthly	June–April

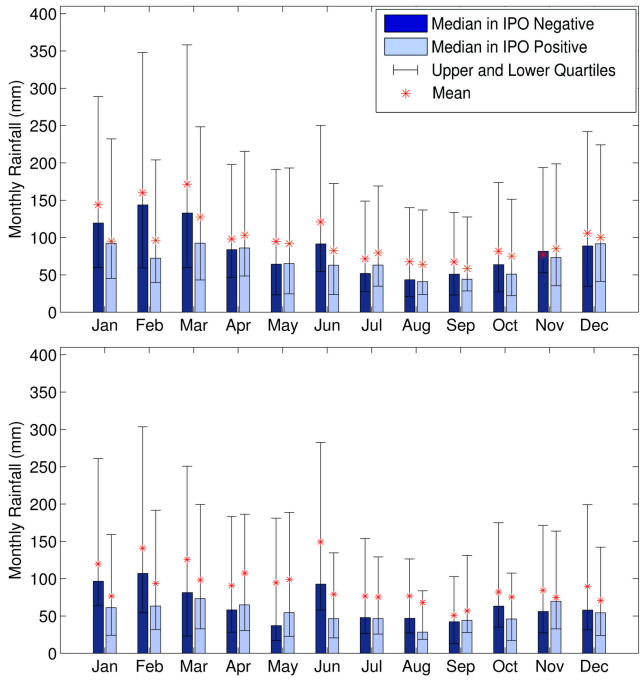

Figure 8. Monthly rainfall statistics at Stroud (upper) and Cataract Dam (lower), data stratified by IPO index.

not between the impact and nonimpact seasons in current or preceding years. At level 1, the short-term process $y_t = [y_{jt} : j = \mathrm{I,NI}]$ refers to the rainfall in both the impact (I) and nonimpact (NI) seasons in year t. The rainfall was simulated using an AR(1) process with Box-Cox (BC) transformation to enable simulation of non-Gaussian data [*Box and Tiao*, 1973] with a shifting mean according to the IPO-PDO state:

$$\begin{aligned} z_{jt} &= \mu_j + \phi_j \times (z_{j(t-1)} - \mu_j) + \epsilon_{jt} \\ \epsilon_{jt} &\sim N(0, \sigma_j^2) \end{aligned}, \tag{3}$$

$$z_{jt} = \begin{cases} \dfrac{y_{jt}^{\lambda_j} - 1}{\lambda_j} & \lambda_j \neq 0 \\ \ln y_{jt} & \lambda_j = 0 \end{cases}, \tag{4}$$

where $y_{j,t}$ is the hydrological data value, $z_{j,t}$ is the transformed value, λ_j is the BC transformation parameter, and j is the season, either impact (I) or nonimpact (NI). The AR(1)-BC parameters μ, ϕ, σ^2, and λ are dependent on the season and IPO-PDO state (w = wet, d = dry).

[38] The model parameters are dependent on the process at level 0, the state of the IPO-PDO during the impact season. A simple relationship between the simulated IPO-PDO state k and the impact season parameters was assumed for the impact season (I):

$$\phi_{\mathrm{I}} = \begin{cases} \phi_{\mathrm{I}d} & \text{if } k_t = d \text{ and } k_{t-1} = d \\ \phi_{\mathrm{I}w} & \text{if } k_t = w \text{ and } k_{t-1} = w \\ 0 & \text{otherwise} \end{cases}, \tag{5}$$

$$\mu_{\mathrm{I}}, \sigma_{\mathrm{I}}, \lambda_{\mathrm{I}} = \begin{cases} \mu_{\mathrm{I}w}, \sigma_{\mathrm{I}w}, \lambda_{\mathrm{I}w} & \text{if } k_t = w \\ \mu_{\mathrm{I}d}, \sigma_{\mathrm{I}d}, \lambda_{\mathrm{I}d} & \text{if } k_t = d \end{cases}. \tag{6}$$

[39] For the nonimpact season (j = NI) there is no hypothesized dependence on the level 0 process and the AR(1)-BC parameters are constants: $\mu_{\mathrm{NI}}, \phi_{\mathrm{NI}}, \sigma_{\mathrm{NI}}, \lambda_{\mathrm{NI}}$.

[40] It is emphasized that only the state of the IPO-PDO is utilized, not the amplitude. This is consistent with the approach of *Kiem et al.* [2003] and *Samuel and Sivapalan* [2008]. A more complex model based on IPO-PDO magnitude is judged not warranted, on account of the relatively low proportion of rainfall variance explained by IPO index values alone.

5.4. CIMSS Framework Calibration Procedure

[41] A Bayesian approach is used to infer the posterior distribution of the CIMSS model parameters. The joint posterior $p(\theta^0, \theta^1 | Y^0_{\mathrm{obs,ins}}, Y^0_{\mathrm{obs,pal}}, Y^1_{\mathrm{obs}})$ combines the elements of the hierarchy. At level 1 of the hierarchy, the formulation of the AR(1)-BC likelihood function for the rainfall process requires the constraint that $z_{jt}\lambda_j + 1 > 0$ to ensure real values for z_{jt}. The approach of *Frost et al.* [2007] was used to implement this constraint in the likelihood function. A minor practical modification was made to take account of the process for y^1_{I} in the impact season. The likelihood expression was evaluated separately for each block of data during positive and negative states of the IPO, since ϕ_{I} takes account of interannual persistence *within* a state, and should influence the change point of states. The ϕ_{I} parameter was found to exhibit similar behavior in both positive and negative IPO-PDO states and as such it was assumed that $\phi_{\mathrm{I}w} = \phi_{\mathrm{I}d}$. A noninformative prior was used for the level 1 parameters. The joint posterior is then:

$$\begin{aligned} &p(\theta^0, \theta^1 | Y^0_{\mathrm{obs,ins}}, Y^0_{\mathrm{obs,pal}}, Y^1_{\mathrm{obs}}) = \\ &\quad p(\theta^0 | Y^0_{\mathrm{obs,ins}}, Y^0_{\mathrm{obs,pal}}) p(\theta^1 | Y^1_{\mathrm{obs}}, Y^0_{\mathrm{obs,ins}}) \\ &\propto p(Y^0_{\mathrm{obs,ins}} | \theta^0) p(Y^0_{\mathrm{obs,pal}} | \theta^0) p(\theta^0) \times p(Y^1_{\mathrm{obs}} | \theta^1, Y^0_{\mathrm{obs,ins}}) p(\theta^1) \end{aligned} \tag{7}$$

with

$$\begin{aligned} \theta^0 &= [\alpha, \beta] \\ \theta^1 &= [\phi_{\mathrm{I}}, \mu_{\mathrm{I}w}, \mu_{\mathrm{I}d}, \sigma_{\mathrm{I}w}, \sigma_{\mathrm{I}d}, \lambda_{\mathrm{I}w}, \lambda_{\mathrm{I}d}, \phi_{\mathrm{NI}}, \mu_{\mathrm{NI}}, \sigma_{\mathrm{NI}}, \lambda_{\mathrm{NI}}]. \end{aligned} \tag{8}$$

[42] The Bayesian approach allows for the evaluation of parameter uncertainty, the importance of which has been well established. For example, in the context of stochastic hydrological models for use in water resource planning, system vulnerability (e.g., water supply drought risk) could be significantly underestimated by approaches that ignore parameter uncertainty [*Stedinger and Taylor*, 1982; *Frost et al.*, 2007]. MCMC methods, such as the Metropolis sampler, can be applied in cases where analytical expressions of the posterior distributions of the parameters are not available. *Frost et al.* [2007], *Gelman et al.* [2004], and *Haario et al.* [2001] give a thorough explanation of the Metropolis algorithm used here.

5.5. Calibration Results

[43] The model was calibrated to rainfall data at the two case study sites on the coast of NSW, Stroud and Cataract Dam. These sites are close to major water supply catchments for the cities of Sydney and Newcastle. In the interests of

brevity, only figures for the Stroud rainfall site calibrated to the IPO-PDO impact season are presented; similar results were obtained for the Cataract Dam site. Analysis of the MCMC parameter samples showed that most of the model parameters had a low correlation, except for α and β. Furthermore, the MCMC convergence diagnostics confirmed the MCMC algorithm had converged after 20,000 function evaluations.

[44] Table 3 shows the mean and standard deviation of the posterior distribution of the parameters for both sites. Figure 9 shows very marked differences between the posterior distributions of mean seasonal rainfall in the wet and dry IPO-PDO states (μ_{Iw} and μ_{Id}). This highlights an additional benefit of evaluating parameter uncertainty, without which it would be harder to determine if the wet and dry state parameters are markedly different. The impact and nonimpact season observed rainfall data was found to be within the 90% probability limits of the simulated data at both sites. The expected values of the mean seasonal rainfall during the IPO-PDO positive state was found to be 15% (156 mm) lower than in the IPO-PDO negative state for the Cataract Dam data, and 28% (123 mm) lower for the Stroud data, during their respective impact seasons.

[45] The differences between the simulated marginal distributions of IPO-PDO positive and negative state impact season rainfall are evident in Figure 10. Two-sided KS tests on the parameter samples of the mean and standard deviation revealed statistically significant differences between the wet and dry distributions ($p < 0.001$ in all cases).

[46] The distributions of 2, 3, 5, 7, 10, 20, and 30 yr overlapping and nonoverlapping accumulated totals of the observed data were found to be consistent with the 90% probability limits of the simulations for both sites. The observed and simulated autocorrelations were also compared within the impact and nonimpact seasons. Again, the observed data was consistent with the 90% probability limits of the simulations.

[47] Figure 11 compares a non-climate-informed model (a seasonal lag-one autoregressive model with Box Cox transformation [AR(1)-BC] [*Thyer et al.*, 2002]) to the distribution of observed annual rainfall at Stroud, using data stratified by the IPO-PDO state. Without the knowledge of the climate mechanism, the AR(1)-BC simulated distribution is a poor fit to the observed distribution within each state. The CIMSS model simulates these two states separately and in doing so captures the observed IPO-PDO positive and negative state distributions. Thus, the climate-informed approach is considered to be preferred over the non-climate-informed AR(1)-BC model.

Table 3. Mean and Standard Deviations of Posterior Distributions of CIMSS Model Parameters Calibrated to Stroud and Cataract Dam Rainfall

	Mean (Standard Deviation)			
Parameter	Stroud		Cataract Dam	
α	1.83	(0.42)	2.16	(0.57)
β	8.60	(2.45)	7.74	(2.46)
μ_{I_w}	432	(34)	1013	(63)
σ_{I_w}	213	(23)	314	(39)
μ_{I_d}	309	(28)	857	(58)
σ_{I_d}	168	(19)	287	(37)
ϕ_I	0.18	(0.10)	0.40	(0.10)
λ_{I_w}	0.52	(0.22)	0.21	(0.17)
λ_{I_d}	0.57	(0.22)	0.26	(0.20)
μ_{NI}	741	(25)	60	(7)
σ_{NI}	220	(17)	71	(9)
ϕ_{NI}	0.15	(0.10)	−0.04	(0.10)
λ_{NI}	0.32	(0.26)	0.13	(0.07)

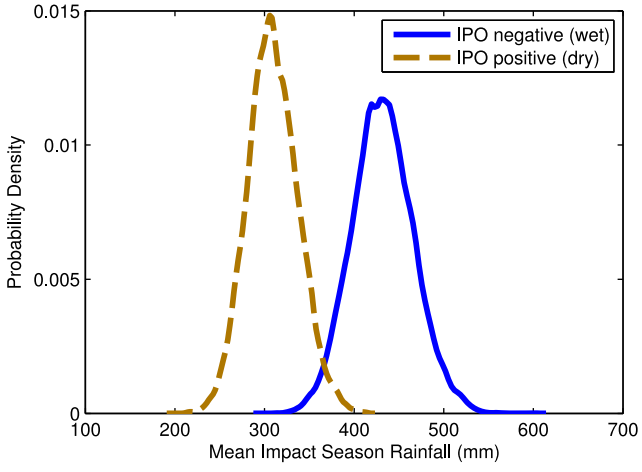

Figure 9. The posterior distributions of mean impact season rainfall in IPO-PDO positive and negative years for Stroud.

[48] Frequency domain characteristics were investigated using the global wavelet power spectrum, as in the work of *Torrence and Compo* [1998] and *Kwon et al.* [2009]. Figure 12a compares the observed and CIMSS simulated wavelet spectra. The observed spectrum was found to be within the model's 90% probability limits as estimated by the Monte Carlo simulation. An almost identical result was obtained for a simple AR(1) model of annual rainfall, similar to the comparison between the WARM and AR(1) models by *Kwon et al.* [2009]. This is further discussed in section 6.3.

6. Discussion

6.1. Challenges of Extracting a Common Climate Signal From Multiple Sources of Paleo Data

[49] This paper has shown that the subjective approach used by *Verdon and Franks* [2006] led to an overestimate

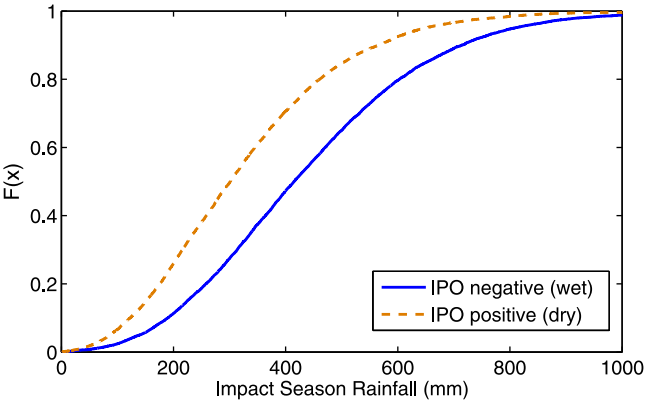

Figure 10. The marginal probability distributions of simulated impact season rainfall at Stroud.

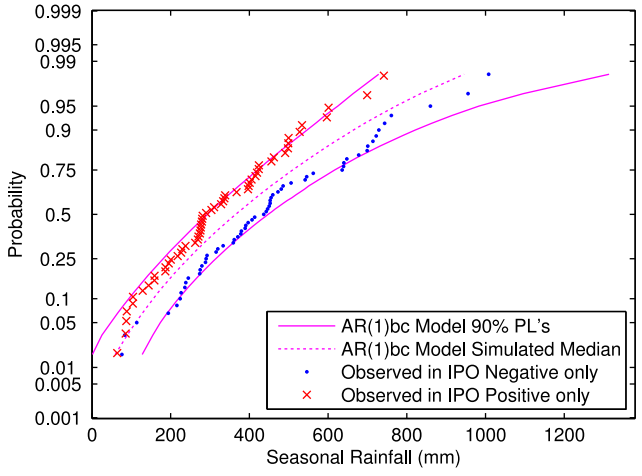

Figure 11. AR(1)-BC-simulated seasonal rainfall distribution compared to observed data in IPO-PDO negative and positive years at Stroud.

of the probability of IPO-PDO run lengths greater than 10 yr. This study's more objective approach resulted in a greater variance in the distribution of run lengths and a higher likelihood of runs of ~10 yr. However, there are significant discrepancies between the published paleo IPO-PDO indices, evident in the low cross correlation between the indices. This is because of a range of issues with paleo data and its interpretation, including possible nonlinearities and errors in the original physical data analysis, nonstationarity of the proxy/climate relationship, and the different levels of explained variance between the various proxies at various locations. These factors need further investigation to ensure that the information content of the paleo data is best utilized. However, to minimize the impacts of these factors, this study filtered the paleo indices in accordance with the best fit to the instrumental IPO data and combined the filtered series using weights that were proportional to the goodness of fit. This approach was not undertaken in the study by *Kwon et al.* [2009] in their combination of multiple proxies; nor in the study by *Prairie et al.* [2008] as it used a single paleo data source. Until further advances are made in combining multiproxy paleoclimate information [e.g., *Haslett et al.*, 2006], the CPIPO index from 1570 to the present provides water resource planners and researchers with a provisional estimate of decadal-scale Pacific climate variability going back ~440 yr.

6.2. Challenges of Combining Paleo and Instrumental Data for Use in Stochastic Hydrological Models: Stationarity and Homogeneity

[50] The CIMSS framework assumes that the random variation in IPO-PDO run lengths and its influence on rainfall is stationary through time. It assumes consistency between the run lengths in the paleo and instrumental periods. The procedure for state classification also assumes that the long-term mean of the paleo series is stationary. Although there is some evidence from paleoclimate studies of nonstationarity in the IPO-PDO phenomenon [*MacDonald and Case*, 2005], other studies highlight the regularity of the oscillations [*Linsley et al.*, 2008]. A KS test at the 5% significance level on the distribution of run lengths between each of the centuries did not reject the assumption of stationarity of the run lengths between centuries. The difference between the inferred posterior distributions of the mean and standard deviation of the IPO-PDO run lengths between the paleo and instrumental period was also computed (Figure 13). The highest probability density region suggests that the mean (standard deviation) of the run lengths for the instrumental data were approximately 2 (2) yr greater than for the paleo data. Nonetheless, the zero difference point lies within the high probability density region. It is therefore concluded that there is insufficient evidence to reject the hypothesis that the paleo and instrumental IPO-PDO run lengths are consistent. There remains a significant research challenge in combining paleo and instrumental data in a manner that allows for nonstationarity in the past. It is noted that decadal predictability is a focus for the upcoming Intergovernmental Panel on

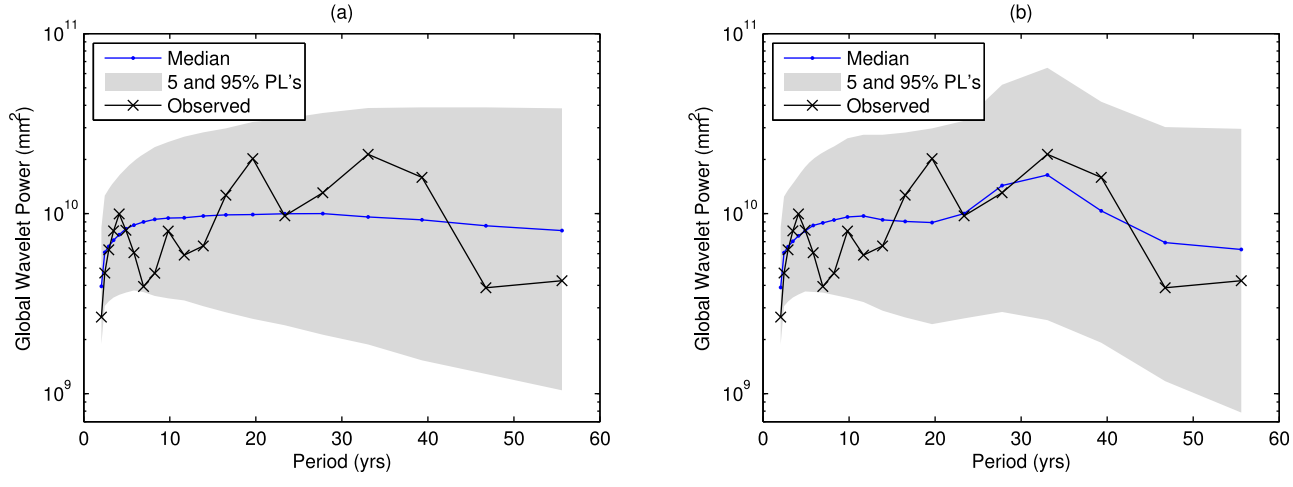

Figure 12. Simulated and observed global wavelet power spectra for annual rainfall at Stroud for (a) CIMSS model with run lengths calibrated to observed and (b) CIMSS model with run length artificially fixed at 16 yrs (which is equivalent to a period of 32 yr).

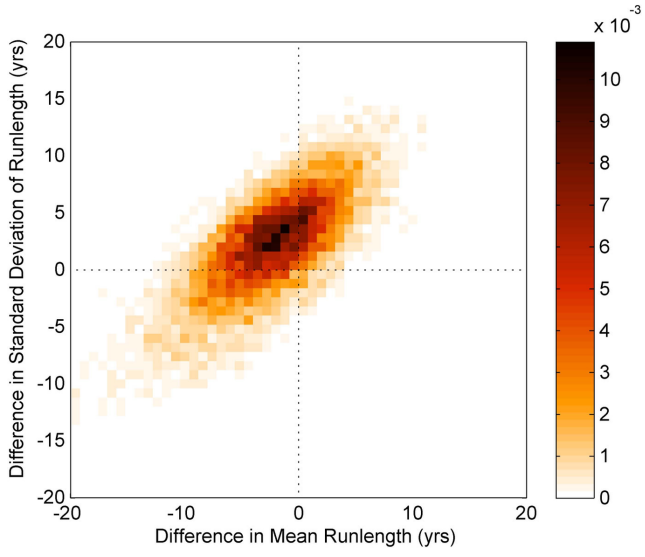

Figure 13. Joint posterior distribution of the mean and standard deviation of the difference between IPO-PDO run lengths inferred from data (paleo minus instrumental).

Climate Change (IPCC) Fifth Assessment Report (AR5) [*Solomon et al.*, 2011; *Taylor et al.*, 2009].

[51] Although this study made the assumption of stationarity in the long term, the rainfall parameters vary on a decadal-scale according to the IPO-PDO. The timescale of these wet and dry periods (as demonstrated on the east coast of Australia) is likely to have significant practical impacts for water resource systems, since most traditional stochastic models do not incorporate this decadal-scale variability.

[52] Some general issues remain with combining paleo and instrumental data. Processing the paleo records necessarily changes the character of the data relative to the instrumental. The uncertainty, because of the noise that is removed through the filtering procedure, is not taken into account in CIMSS model simulations. The assumption was made that the paleo and instrumental data are homogeneous, and that run lengths from paleo and instrumental data have equal weight, despite paleo and instrumental data being derived from different sources and paleo records being subject to greater uncertainty. The method used in this study to combine the paleo records sought to reduce the impact of these assumptions. It is noted that these issues apply to earlier studies by *Kwon et al.* [2009] and *Prairie et al.* [2008].

[53] These considerations suggest that future research should focus on methods that better take into account the additional uncertainty in the paleo data. For example, one approach would be to add a random noise term to the paleo run length sequences with the characteristics of this noise calibrated to the instrumental record.

6.3. Challenges of Statistically Assessing Long-Term Variability

[54] It is hypothesized that the flatness of the spectrum of the CIMSS model in Figure 12a is due to the high variability of simulated IPO-PDO run lengths. To test this hypothesis, run lengths were artificially set to precisely 16 yr. The resulting wavelet spectrum in Figure 12b shows a peak at a period of ~32 yr (equivalent to a run length of 16 yr). This confirms the hypothesis that the flat rainfall spectrum was probably due to the high variance in simulated run lengths, which was in turn due to the variability in the observed paleo and instrumental IPO-PDO run lengths and the incorporation of parameter uncertainty, rather than a shortcoming in the modeling approach.

6.4. Extensions to the CIMSS Framework: Incorporating Other Climate Processes and Multisite Analysis

[55] An unresolved question in the climate literature [*Meinke et al.*, 2005] is whether the low frequency variability represented as the IPO or PDO is an artifact of stochastic variability of ENSO and/or other mechanisms [*Newman et al.*, 2003; *Schneider and Cornuelle*, 2005; *Power et al.*, 2006] or, in fact, an independent dynamical climate mode [*Folland et al.*, 2002; *Cobb et al.*, 2003; *Parker et al.*, 2007]. Regardless of the cause and effect status of the large-scale oscillations of Pacific climate, this study exploited the association between rainfall and IPO-PDO indices to inform stochastic rainfall simulation.

[56] Climate modes such as the IPO-PDO, ENSO, IOD, and SAM and the impacts of climate change have different spatial and temporal effects on hydrological processes. For example, ENSO impacts are more intense and ENSO typically explains a greater proportion of the overall variability in hydrological data than other mechanisms. However, the IPO-PDO has much longer run lengths, the likely practical impacts of which are discussed in section 6.5.

[57] Studies by *Cai et al.* [2010] and *Power et al.* [1999] discussed the asymmetry between the ENSO-rainfall teleconnection, with the La Niña-rainfall relationship being more closely linked to the La Niña amplitude than the El Niño-rainfall relationship is to the El Niño amplitude. The connection between the amplitude of ENSO events and rainfall is associated with the IPO-PDO, with the IPO-PDO positive state leading to a breakdown in the asymmetry in the pre-1950 and pre-1980 IPO-PDO positive states. Future work to model this would require explicit modeling of the oscillations of ENSO, rather than just the IPO-PDO state run lengths as used here. Possible model formulations would be to have ENSO event frequency varying with the IPO-PDO [*Kiem et al.*, 2003] or the variability of the asymmetry of ENSO impacts [*Cai et al.*, 2010; *Power et al.*, 1999] being simulated on a decadal timescale. A detailed investigation of the temporal and spatial IPO-PDO-ENSO impacts would aid the construction of such a model.

[58] Modeling the interaction of climate modes remains a challenge, in particular when using a categorical methodology. This is because the short instrumental record limits the number of combinations of multiple climate mode states (e.g., El Niño and IOD positive) sampled in the instrumental record. Advances in paleoclimate reconstructions would provide improved understanding of the dynamics of these modes and their interactions. The method used in this paper to calibrate filters directly from various paleo data sources to a target instrumental signal is an objective approach that could be applied to combine other paleo data sources, and hence possibly provide greater certainty around the interaction of climate modes. The appropriate incorporation of other climate modes is left to future work.

[59] The CIMSS framework was used here to incorporate climate variability into stochastic simulations of hydrological data at a single site; however, the approach could be extended to multisite simulation using a Bayesian hierarchical modeling (BHM) approach similar to those used by *Frost et al.* [2007], *Lima and Lall* [2009], and *Kwon et al.* [2009]. Previous BHM methods such as *Kwon et al.* [2009] have assumed a constant standard deviation for seasonal rainfall in different climate states. However, there were differences of 27% and 9% in the expected value of the posteriors for the standard deviation of seasonal rainfall at Stroud and Cataract Dam respectively (σ_{I_w} and σ_{I_d} in Table 3). This illustrates the importance of incorporating the influence of climate mechanisms on the variance of rainfall processes in stochastic hydrological models.

[60] This study defined the IPO-PDO impact season as the contiguous sequence of months with a maximum statistically significant difference (at the 5% significance level) between IPO-PDO stratified rainfall totals. This resulted in differences between the impact seasons at the two case study sites. Nonetheless, a fairly robust trend across the 47 coastal sites, with summer centered impact seasons, was identified. Several issues might be masking an otherwise distinct sequence of months where the IPO-PDO has an impact over a wide area, including the limitation to just one impact season, the influence of the significance level threshold on season choice, the limitation to contiguous sequences of months, high rainfall variability generally, and possibly uncertainty in the IPO-PDO indices. For example, the strong IPO-PDO impact in June at Cataract Dam (Figure 8) appears to be the reason for its much longer impact season (June–April), compared to Stroud (January–March). *Folland et al.* [2002] used data from November–April in their study of the impact of the IPO-PDO on SPCZ location because that is the period when the SPCZ is most active. SPCZ activity could be used to inform the ENSO or IPO-PDO impact season choice in future work. Although the impact season choice was data-driven in this study, for future work a probabilistic method for simulating the impact season would be preferred over an a priori deterministic method. For example, the impact season could be drawn from a probability distribution of all monthly sequences with statistically significant differences between rainfall totals stratified by IPO-PDO (or other climate mechanisms). In a multisite simulation context, a consistent methodology would need to be defined for the simulation of impact seasons across sites.

6.5. Practical Implications for Water Supply Security

[61] Figure 11 showed that traditional non-climate-informed models (such as the AR(1) model) are unlikely to account for the influence of climate mechanisms such as the IPO-PDO. Future work will investigate the impact of climate modes on drought risk to water supply systems. Such analyses could provide insights into appropriate adaptive management strategies and long-term planning decisions for water supply systems.

[62] The incorporation of parameter uncertainty helps to improve the reliability of stochastic simulations. Approaches such as those of *Samuel and Sivapalan* [2008], *Prairie et al.* [2008] and *Kwon et al.* [2009] (in the WARM component of their rainfall model) that do not incorporate parameter uncertainty in their simulations are likely to underestimate the variability in predictions. In doing so, these approaches possibly underestimate the resulting drought (or flood) risk and overestimate system reliability, as highlighted by *Stedinger and Taylor* [1982].

7. Conclusions

[63] A general climate-informed multi-time scale stochastic (CIMSS) framework was presented in which stochastic models of recognized climate mechanisms are used to condition stochastic hydrological models. A two level hierarchy was chosen to illustrate the framework, with the upper level focusing on decadal-scale variability. Paleo and instrumental data were used to identify the variability at the top level. The lower level of the hierarchy was a stochastic rainfall model with parameters conditioned on the decadal-scale variability at the top level. The development of this model led to the following conclusions:

[64] 1. It was shown that the subjective choice of a 30-yr window in the study by *Verdon and Franks* [2006] led to an overestimation of the run lengths of states of the IPO-PDO. The adaptive method used in this paper to fit filters to the contributing signals avoided the need to subjectively choose a shift detection window width. Furthermore, the need to make subjective choices to estimate the history of crossings from multiple paleo proxies was avoided by combining the signals by weighting by the goodness of fit to the instrumental data. A new combined paleo IPO-PDO (CPIPO) signal was produced from seven IPO-PDO paleo sources, dating back ~440 yr. The analysis gave improved certainty regarding the distribution of IPO-PDO run lengths. Nonetheless, significant uncertainty remains.

[65] 2. Model selection using the BIC on the paleo runs favored a gamma model over the Markov chain model (MCM) for IPO-PDO run lengths. The Markov chain family of models is structurally deficient in this context because the mode of the run length distribution is always located at a run length of 1. This means the MCM overestimates the proportion of shorter IPO-PDO runs (e.g., 1–5 yr) and underestimates the proportion of longer IPO-PDO runs. The MCM and related models have been widely used to simulate wet/dry climate states [*Thyer and Kuczera*, 2000; *Lambert et al.*, 2003; *Akintug and Rasmussen*, 2005; *Frost et al.*, 2007; *Samuel and Sivapalan*, 2008; *Prairie et al.*, 2008]. This study shows that these types of models are a poor choice for modeling the wet/dry state run lengths of decadal variability, such as the IPO-PDO phenomenon.

[66] 3. A two-level CIMSS framework was applied to two rainfall data case study sites on the east coast of NSW, Australia. The upper level consisted of a gamma model for the IPO-PDO state run lengths. This was calibrated to the run lengths of the CPIPO and the instrumental IPO index. Seasonal rainfall was modeled at the lower level with an autoregressive model with Box-Cox transformation. An MCMC calibration routine was utilized to quantify parameter uncertainty and incorporate that uncertainty into the hydrological simulations. The model was found to replicate observed statistics such as the seasonal, annual, and multiyear accumulated rainfall distributions and interannual autocorrelations. In comparison, a non-climate-informed (the AR(1)-BC) model was found to produce a poor fit to observed data within

each state of the IPO-PDO. Thus, the CIMSS approach is preferred over the non-climate-informed model.

[67] 4. The findings of this study are based on the assumption of stationarity between the paleo and instrumental IPO-PDO data. While statistical tests do not reject this assumption, more research is needed to better inform such work.

[68] 5. Persistent states of the IPO-PDO lasting for a decade or more could increase the vulnerability of water supply reservoir systems to drought. Drought risk simulations that are uninformed of climate processes could under- (or over-) estimate drought risk as the IPO-PDO states change. This could place into question planning decisions that were based on traditional non-climate-informed stochastic models. Future work will utilize the climate-informed approach to assess the impact of longer-term climate variability on water supply drought risk. The model presented in this study enables the quantification of risks to water supply systems due to intrinsic modes of climate variability. This will help to provide more reliable estimates of system vulnerability and an important baseline against which the risks due to climate change can be compared.

[69] **Acknowledgments.** The authors wish to thank Chris Folland (Hadley Centre, UKMO) and the Australian Bureau of Meteorology for data. The authors gratefully acknowledge the financial support from an Australian Research Council linkage grant with Hunter Water Corporation. In addition, the authors gratefully acknowledge the contribution of Dmitri Kavetski, the primary author of DMSL, a library of numerical algorithms and utilities coded in Fortran-95. The routines from DMSL were used in analyses undertaken in this paper. The wavelet software was provided by C. Torrence and G. Compo, and is available at http://atoc.colorado.edu/research/wavelets/. The CPIPO data is available via email request from the first or second authors: Ben Henley (ben.henley@uon.edu.au) or Mark Thyer (mthyer@civeng.adelaide.edu.au).

References

Akintug, B., and P. F. Rasmussen (2005), A Markov switching model for annual hydrologic time series, *Water Resour. Res.*, *41*(9), W09424, doi:10.1029/2004WR003605.

Allan, R., J. Lindsay, and D. Parker (1996), *El Nino Southern Oscillation and Climatic Variability*, 405 pp., CSIRO Publishing, Collingwood, Australia.

Arblaster, J. M., G. A. Meehl, and A. M. Moore (2002), Interdecadal modulation of Australian rainfall, *Clim. Dyn.*, *18*(6), 519–531.

Arguez, A., P. Yu, and J. J. O'Brien (2008), A new method for time series filtering near endpoints, *J. Atmos. Oceanic Technol.*, *25*(4), 534–546.

Biondi, F., A. Gershunov, and D. R. Cayan (2001), North Pacific decadal climate variability since 1661, *J. Clim.*, *14*, 5–10.

Box, G., and G. Tiao (1973), *Bayesian Inference in Statistical Analysis*, 588 pp., Addison-Wesley, Reading, Mass.

Cai, W. J., P. van Rensch, T. Cowan, and A. Sullivan (2010), Asymmetry in ENSO Teleconnection with Regional Rainfall, Its Multidecadal Variability, and Impact, *J. Clim.*, *23*(18), 4944–4955, doi:10.1175/2010JCLI3501.1.

Cobb, K. M., C. D. Charles, H. Cheng, and R. L. Edwards (2003), El Nino/Southern Oscillation and tropical Pacific climate during the last millennium, *Nature*, *424*(6946), 271–276.

D'Arrigo, R., and R. Wilson (2006), On the Asian expression of the PDO, *Int. J. Climatol.*, *26*(12), 1607–1617.

D'Arrigo, R., R. Villalba, and G. Wiles (2001), Tree-ring estimates of Pacific decadal climate variability, *Clim. Dyn.*, *18*(3), 219–224.

Folland, C. K., J. A. Renwick, M. J. Salinger, and A. B. Mullan (2002), Relative influences of the Interdecadal Pacific Oscillation and ENSO on the South Pacific convergence zone, *Geophys. Res. Lett.*, *29*(13), 1643, doi:10.1029/2001GL014201.

Frost, A. J., M. A. Thyer, R. Srikanthan, and G. Kuczera (2007), A general Bayesian framework for calibrating and evaluating stochastic models of annual multi-site hydrological data, *J. Hydrol.*, *340*(3–4), 129–148, doi:10.1016/j.jhydrol.2007.03.023.

Gedalof, Z., and D. J. Smith (2001), Interdecadal climate variability and regime-scale shifts in Pacific North America, *Geophys. Res. Lett.*, *28*, 1515–1518.

Gelman, A., J. Carlin, H. Stern, and D. Rubin (2004), *Bayesian Data Analysis*, 2nd ed., 696 pp., Chapman and Hall, Fla.

Haario, H., E. Saksman, and J. Tamminen (2001), An adaptive Metropolis algorithm, *Bernoulli*, *7*(2), 223–242.

Haslett, J., M. Whiley, S. Bhattacharya, M. Salter-Townshend, S. P. Wilson, J. R. M. Allen, B. Huntley, and F. J. G. Mitchell (2006), Bayesian palaeoclimate reconstruction, *J. R. Stat. Soc. Ser. A*, *169*, 395–430.

Heinrich, I., K. Weidner, G. Helle, H. Vos, J. Lindesay, and J. C. G. Banks (2009), Interdecadal modulation of the relationship between ENSO, IPO and precipitation: Insights from tree rings in Australia, *Clim. Dyn.*, *33*(1), 63–73.

Hendon, H. H., D. W. J. Thompson, and M. C. Wheeler (2007), Australian rainfall and surface temperature variations associated with the Southern Hemisphere annular mode, *J. Clim.*, *20*(11), 2452–2467.

Kiem, A. S., and S. W. Franks (2004), Multi-decadal variability of drought risk, Eastern Australia, *Hydrol. Processes*, *18*(11), 2039–2050.

Kiem, A. S., S. W. Franks, and G. Kuczera (2003), Multi-decadal variability of flood risk, *Geophys. Res. Lett.*, *30*(2), 1035, doi:10.1029/2002GL015992.

Koutsoyiannis, D. (2000), A generalized mathematical framework for stochastic simulation and forecast of hydrologic time series, *Water Resour. Res.*, *36*(6), 1519–1533.

Kwon, H. H., U. Lall, and J. Obeysekera (2009), Simulation of daily rainfall scenarios with interannual and multidecadal climate cycles for South Florida, *Stochastic Environmental Research and Risk Assessment*, *23*(7), 879–896, doi:10.1007/s00477-008-0270-2.

Lambert, M. F., J. P. Whiting, and A. V. Metcalfe (2003), A non-parametric hidden Markov model for climate state identification, *Hydrol. Earth Syst. Sci.*, *7*(5), 652–667.

Lavery, B., G. Joung, and N. Nicholls (1997), An extended high-quality historical rainfall dataset for Australia, *Australian Meteorological Magazine*, *46*(1), 27–38.

Lima, C. H. R., and U. Lall (2009), Hierarchical Bayesian modeling of multisite daily rainfall occurrence: Rainy season onset, peak, and end, *Water Resour. Res.*, *45*, W07422, doi:10.1029/2008WR007485.

Linsley, B., G. Wellington, and D. Schrag (2000), Decadal sea surface temperature variability in the sub-tropical South Pacific from 1726 to 1997 A.D., *Science*, *290*, 1145–1148.

Linsley, B. K., P. P. Zhang, A. Kaplan, S. S. Howe, and G. M. Wellington (2008), Interdecadal-decadal climate variability from multicoral oxygen isotope records in the South Pacific Convergence Zone region since 1650 A.D., *Paleoceanography*, *23*(2), PA2219, doi:10.1029/2007PA001539.

MacDonald, G. M., and R. A. Case (2005), Variations in the Pacific Decadal Oscillation over the past millennium, *Geophys. Res. Lett.*, *32*(8), L08703, doi:10.1029/2005GL022478.

Mann, M. E. (2004), On smoothing potentially non-stationary climate time series, *Geophys. Res. Lett.*, *31*(7), L07214, doi:10.1029/2004GL019569.

Mann, M. E. (2009), Defining dangerous anthropogenic interference, *Proc. Natl. Acad. Sci. U. S. A.*, *106*(11), 4065–4066.

Mantua, N. J., S. R. Hare, Y. Zhang, J. M. Wallace, and R. C. Francis (1997), A Pacific interdecadal climate oscillation with impacts on salmon production, *Bull. Am. Meteorol. Soc.*, *78*(6), 1069–1079.

Mauget, S. A. (2003), Multidecadal regime shifts in US streamflow, precipitation, and temperature at the end of the twentieth century, *J. Clim.*, *16*(23), 3905–3916.

McBride, J., and N. Nicholls (1983), Seasonal Relationships between Australian Rainfall and the Southern Oscillation, *Mon. Weather Rev.*, *111*(10), 1998–2004, http://dx.doi.org/10.1175.

McGowan, H. A., S. K. Marx, J. Denholm, J. Soderholm, and B. S. Kamber (2009), Reconstructing annual inflows to the headwater catchments of the Murray River, Australia, using the Pacific Decadal Oscillation, *Geophys. Res. Lett.*, *36*, L06707, doi:10.1029/2008GL037049.

McGregor, S., A. Timmermann, and O. Timm (2010), A unified proxy for ENSO and PDO variability since 1650, *Climate of the Past*, *6*(1), 1–17.

Mehrotra, R., and A. Sharma (2007), Preserving low-frequency variability in generated daily rainfall sequences, *J. Hydrol.*, *345*(1–2), 102–120.

Meinke, H., P. deVoil, G. L. Hammer, S. Power, R. Allan, R. C. Stone, C. Folland, and A. Potgieter (2005), Rainfall variability at decadal and longer time scales: Signal or noise?, *J. Clim.*, *18*(1), 89–96.

Meneghini, B., I. Simmonds, and I. N. Smith (2007), Association between Australian rainfall and the southern annular mode, *Int. J. Clim.*, *27*(1), 109–121.

Micevski, T., S. W. Franks, and G. Kuczera (2006), Multidecadal variability in coastal eastern Australian flood data, *J. Hydrol.*, *327*(1–2), 219–225.

Newman, M., G. P. Compo, and M. A. Alexander (2003), ENSO-forced variability of the Pacific decadal oscillation, *J. Clim.*, *16*(23), 3853–3857.

Parker, D., C. Folland, A. Scaife, J. Knight, A. Colman, P. Baines, and B. Dong (2007), Decadal to multidecadal variability and the climate change background, *J. Geophys. Res.*, *112*, D18115, doi:10.1029/2007JD008411.

Potter, N. J., F. H. S. Chiew, and A. J. Frost (2010), An assessment of the severity of recent reductions in rainfall and runoff in the Murray-Darling Basin, *J. Hydrol.*, *381*(1–2), 52–64, doi:10.1016/j.jhydrol.2009.11.025.

Power, S., T. Casey, C. Folland, A. Colman, and V. Mehta (1999), Inter-decadal modulation of the impact of ENSO on Australia, *Clim. Dyn.*, *15*(5), 319–324.

Power, S., M. Haylock, R. Colman, and X. D. Wang (2006), The predictability of interdecadal changes in ENSO activity and ENSO teleconnections, *J. Clim.*, *19*(19), 4755–4771.

Prairie, J., K. Nowak, B. Rajagopalan, U. Lall, and T. Fulp (2008), A stochastic nonparametric approach for streamflow generation combining observational and paleoreconstructed data, *Water Resour. Res.*, *44*(6), W06423, doi:10.1029/2007WR006684.

Rayner, N. A., P. Brohan, D. E. Parker, C. K. Folland, J. J. Kennedy, M. Vanicek, T. J. Ansell, and S. F. B. Tett (2006), Improved analyses of changes and uncertainties in sea surface temperature measured in situ since the mid-nineteenth century: The HadSST2 data set, *J. Clim.*, *19*(3), 446–469.

Saji, N. H., B. N. Goswami, P. N. Vinayachandran, and T. Yamagata (1999), A dipole mode in the tropical Indian Ocean, *Nature*, *401*(6751), 360–363.

Salas, J. D. (1993), Analysis and modeling of hydrologic time series, in *Handbook of Hydrology*, edited by D. R. Maidment, pp. 19.1–19.72, McGraw-Hill, New York.

Samuel, J. M., and M. Sivapalan (2008), A comparative modeling analysis of multiscale temporal variability of rainfall in Australia, *Water Resour. Res.*, *44*, W07401, doi:10.1029/2007WR006373.

Schneider, N., and B. D. Cornuelle (2005), The forcing of the Pacific Decadal Oscillation, *J. Clim.*, *18*(21), 4355–4373, available at http://dx.doi.org/10.1175.

Schwarz, G. (1978), Estimating the dimension of a model, *Ann. Stat.*, *6*(2), 461–464.

Sharma, A., D. G. Tarboton, and U. Lall (1997), Streamflow simulation: A nonparametric approach, *Water Resour. Res.*, *33*(2), 291–308.

Shen, C. M., W. C. Wang, W. Gong, and Z. X. Hao (2006), A Pacific Decadal Oscillation record since 1470 AD reconstructed from proxy data of summer rainfall over eastern China, *Geophys. Res. Lett.*, *33*(3), L03702, doi:10.1029/2005GL024804.

Solomon, A., L. Goddard, A. Kumar, J. Carton, C. Deser, I. Fukumori, A. M. Greene, G. Hererl, B. Kirtman, Y. Kushnir, et al. (2011), Distinguishing the Roles of Natural and Anthropogenically Forced Decadal Climate Variability: Implication for Prediction, *Bull. Am. Meteorol. Soc.*, *92*(2), doi:10.1175/2010BAMS2962.1.

Soon, W. W. H., D. R. Legates, and S. L. Baliunas (2004), Estimation and representation of long-term (greater than 40 year) trends of Northern-Hemisphere-gridded surface temperature: A note of caution, *Geophys. Res. Lett.*, *31*(3), L03209, doi:10.1029/2003GL019141.

Speer, M. S. (2008), On the late twentieth century decrease in Australian east coast rainfall extremes, *Atmos. Sci. Lett.*, *9*(3), 160–170.

Stedinger, J. R., and M. R. Taylor (1982), Synthetic streamflow generation 2. Effect of parameter uncertainty, *Water Resour. Res.*, *18*(4), 919–924.

Taylor, K. E., R. J. Stouffer, and G. A. Meehl (2009), A summary of the CMIP5 experimental design, *Tech. rep.*, CLIVAR, available at http://www-pcmdi.llnl.gov/.

Thyer, M., and G. Kuczera (2000), Modeling long-term persistence in hydroclimatic time series using a hidden state Markov model, *Water Resour. Res.*, *36*(11), 3301–3310.

Thyer, M., and G. Kuczera (2003), A hidden Markov model for modelling long-term persistence in multi-site rainfall time series 1. Model calibration using a Bayesian approach, *J. Hydrol.*, *275*(1–2), 12–26.

Thyer, M., G. Kuczera, and Q. J. Wang (2002), Quantifying parameter uncertainty in stochastic models using the Box-Cox transformation, *J. Hydrol.*, *265*(1–4), 246–257.

Thyer, M., A. J. Frost, and G. Kuczera (2006), Parameter estimation and model identification for stochastic models of annual hydrological data: Is the observed record long enough?, *J. Hydrol.*, *330*(1–2), 313–328.

Tome, A. R., and P. M. A. Miranda (2005), Continuous partial trends and low-frequency oscillations of time series, *Nonlinear Processes in Geophysics*, *12*(4), 451–460.

Torrence, C., and G. P. Compo (1998), A practical guide to wavelet analysis, *Bull. Am. Meteorol. Soc.*, *79*(1), 61–78.

Ummenhofer, C. C., M. H. England, P. C. McIntosh, G. A. Meyers, M. J. Pook, J. S. Risbey, A. S. Gupta, and A. S. Taschetto (2009), What causes southeast Australia's worst droughts?, *Geophys. Res. Lett.*, *36*, L04706, doi:10.1029/2008GL036801.

Verdon, D. C. (2007), Pacific and Indian Ocean climate variability: Implications for water resource management in Eastern Australia, Ph.D. thesis, Univ. of Newcastle, Australia.

Verdon, D. C., and S. W. Franks (2006), Long-term behaviour of ENSO: Interactions with the PDO over the past 400 years inferred from paleoclimate records, *Geophys. Res. Lett.*, *33*(6), L06712, doi:10.1029/2005GL025052.

Verdon, D., and S. Franks (2007), Long-term drought risk assessment in the Lachlan River Valley—A paleoclimate perspective, *Aust. J. Water Resour.*, *11*(2), 145.

Verdon, D. C., A. M. Wyatt, A. S. Kiem, and S. W. Franks (2004), Multidecadal variability of rainfall and streamflow: Eastern Australia, *Water Resour. Res.*, *40*(10), W10201, doi:10.1029/2004WR003234.

Verdon-Kidd, D. C., and A. S. Kiem (2009), On the relationship between large-scale climate modes and regional synoptic patterns that drive Victorian rainfall, *Hydrol. Earth Syst. Sci.*, *13*(4), 467–479.

Vörösmarty, C. J., P. Green, J. Salisbury, and R. B. Lammers (2000), Global water resources: Vulnerability from climate change and population growth, *Science*, *289*(5477), 284–288, doi:10.1126/science.289.5477.284.

Westra, S., and A. Sharma (2009), Probabilistic estimation of multivariate streamflow using independent component analysis and climate information, *J. Hydrometeorol.*, *10*(6), 1479–1492, doi:10.1175/2009JHM1121.1.

Whiting, J. P., M. F. Lambert, and A. V. Metcalfe (2003), Modelling persistence in annual Australian point rainfall, *Hydrol. Earth Syst. Sci.*, *7*(2), 197–211.

Zhang, Y., J. M. Wallace, and D. S. Battisti (1997), ENSO-like interdecadal variability: 1900–93, *J. Clim.*, *10*(5), 1004–1020.

S. W. Franks, B. J. Henley, and G. Kuczera, Discipline of Civil, Surveying and Environmental Engineering, University of Newcastle, University Drive, Callaghan NSW 2308, Australia. (ben.henley@uon.edu.au)

M. A. Thyer, School of Civil, Environmental and Mining Engineering, University of Adelaide, North Terrace, Adelaide SA 5005, Australia.